Combustion and Flame 158 (2011) 1970–1976

Contents lists available at ScienceDirect

Combustion and Flame

journal homepage: www.elsevier.com/locate/combustflame

Characterization of flame radiosity in shrubland fires

Miguel G. Cruz [a,*], Bret W. Butler [b], Domingos X. Viegas [c], Pedro Palheiro [d]

[a] Bushfire Dynamics and Applications, CSIRO Ecosystem Sciences and Climate Adaptation Flagship, GPO Box 284, Canberra, ACT 2601, Australia
[b] US Forest Service, Rocky Mountain Research Station, Fire Sciences Laboratory, 5775 Hwy. 10 W, Missoula, MT, USA
[c] Department of Mechanical Engineering, University of Coimbra, Polo II, Pinhal de Marrocos, 3030 Coimbra, Portugal
[d] Autoridade Florestal Nacional, COTF, Chã do Freixo, 3200-901 Lousã, Portugal

ARTICLE INFO

Article history:
Received 5 October 2010
Received in revised form 17 February 2011
Accepted 4 March 2011
Available online 28 March 2011

Keywords:
Fire behaviour
Fire spread
Experimental fire
Flame radiation
Flame temperature

ABSTRACT

The present study is aimed at quantifying the flame radiosity vertical profile and gas temperature in moderate to high intensity spreading fires in shrubland fuels. We report on the results from 11 experimental fires conducted over a range of fire rate of spread and frontal fire intensity varying respectively between 0.04–0.35 m s^{-1} and 468–14,973 kW m^{-1}. Flame radiosity, or radiant emissive power, and gas temperatures were measured with narrow angle radiometers and fine wire thermocouples located at three different heights in the flames, 0.6, 1.1 and 1.6 m above ground. Measured peak radiosity within the visual flame region (reaction zone and free flame) varied between 41 and 176 kW m^{-2}. Measurements within the intermittent flame region above the visually estimated average flame height varied between 10 and 30 kW m^{-2}. The flame vertical radiometric profile was characterized by a uniform area within the reaction zone and lower free flame, and a decrease in radiosity with height as the measurements approach the flame tip.

1. Introduction

Fire behaviour modelling aims at developing tools that can be used to support fire management decision-making and increase our understanding of fire phenomena. Recent advances in fire behaviour modelling have applied numerical methods to the theoretical analysis of transport processes involved in a fire [1–4]. The fundamental description of fire and atmospheric dynamics processes give these models the potential to fully describe the spread of fires. Knowledge of the thermal radiation produced in the combustion of gaseous fuels in spreading fires and its contribution to the preheating of unburned fuels is an important component of these models [5,6]. Nevertheless, our understanding of the fundamental properties of flames, such as, fluid temperature, radiosity and nonsteady behaviour in wildland fires, is largely incomplete.

Experimental fires conducted under controlled laboratory conditions have been a source of detailed measurements of flame geometry [7], fluid temperature and velocity [8,9], emissivity [10] and radiosity, or radiant emissive power, the total energy radiated per unit area per unit time, [11]. Of relevance to the present study is the description of flame vertical radiometric profile from free burning fires by Wotton et al. [11]. Using narrow angle radiometers [12] these authors quantified the vertical variation in the radiative properties of flames in fires spreading under no-wind conditions. Radiation from the free flame was observed to decay with height in the flame. The scale of [11] experiments still limit the type of inferences that can be made regarding the behaviour of high intensity flames, as laboratory fires cannot replicate the fuel consumption rates, flame size, radiative heat fluxes, flow velocities and turbulence observed in outdoor fires [13,14]. Acquiring such flame information presents a challenge, due to the safety and operational constrains associated with conducting outdoor fire experiments and the technical difficulties in instrumenting a free spreading fire. The harsh environment associated with wildland fire also limits the type of sensors that can be used with minimal effect on flame structure. Butler et al. [15] measured flame temperatures and radiant emissive power in a number of crown fire experiments in Northern Canada [16]. Radiant emissive power measured in these fires were more than double those of [11]. Butler et al. [15] observed a flat radiometric profile within the forest stand (sub-canopy and canopy space), which can be viewed as an extended reaction zone for crown fire flames [17]. Other studies conducted point measurements of radiant heat fluxes in shrubland fires [14,18].

The objective of the present study was to measure the radiosity and gas temperatures of flames spreading in shrubland vegetation, and understand how such quantities vary with flame structure and how they are linked with measures of fire behaviour.

* Corresponding author. Address: Bushfire Dynamics and Applications, CSIRO Ecosystem Sciences and Climate Adaptation Flagship, GPO Box 284, Canberra, ACT 2601, Australia.
E-mail address: miguel.cruz@csiro.au (M.G. Cruz).

0010-2180/$ - see front matter Crown Copyright © 2011 Published by Elsevier Inc. on behalf of The Combustion Institute. All rights reserved.
doi:10.1016/j.combustflame.2011.03.002

2. Experimental methods

2.1. Site characteristics and fuel complex

The measurements were collected as part of a multi-year experimental burning program designed to characterize wind and slope effects on fire behaviour in shrubland fuel complexes. Information regarding the experimental burning program can be found in [19]. The sites are located in the Lousã mountain range (40°15′N, 8°10′W) in Central Portugal, with Gestosa located at an altitude of 700–800 m ASL, and Gondramaz at 850 m ASL. Average plot size and fireline width were respectively 2500 m^2 and 55 m. The experimental area vegetation consists of continuous (close to 100% cover) shrublands dominated by the following species: *Erica umbellata*, *Erica australis* and *Chamaespartium tridentatum*. Fuelbed structure was determined by double sampling techniques [20]. Destructive sampling of shrub fuels was aimed at determining fuel load and bulk density by fuel particle size class and state (live or dead) per species. As a note, the terms fuel and vegetation are used interchangeably here. The linear transect method [21] was used to estimate composition, percent coverage, height, and volume by species in each burn plot. Fuel age (time since last fire) varied between 16 and 20 years. Average fine fuel load (dead fuels with diameter less then 6 mm and live fuels with diameter less than 3 mm) per plot within the shrub canopy averaged 1.4 kg m^{-2} at Gestosa and 0.77 kg m^{-2} at Gondramaz (Table 1). The litter layer in this fuel complex is incipient, and does not sustain fire propagation [22,23]. Live vegetation accounts for 79% of the fuel load in Gestosa and 72% in Gondramaz. Average fuel bed height was 0.97 m in Gestosa and 0.29 m in Gondramaz. Canopy bulk density averaged 1.44 kg m^{-3} in Gestosa and 2.61 kg m^{-3} in Gondramaz. Further information on fire behaviour dynamics in this vegetative complex can be found in [23].

2.2. Weather and fuel moisture sampling

Wind speed and direction (6 m above ground in the open), precipitation, temperature and relative humidity were recorded by a network of three automatic weather stations positioned within the experimental area. The weather stations were located so that their measurements were not influenced by fire-generated flow. Collection of hourly observations started 2 months prior to the experimental burns. During burns weather data consisted of 1 min averages. Fuel moisture (percent mass/oven dry mass) samples were collected prior to ignition for each experimental fire. Five samples were collected per dominant species and state, i.e., fine live and dead fuels. Live fuel moisture sampling included foliage and small twigs (diameter less than 3 mm) of the dominant species. Fuel moisture samples were oven dried at nominally 100 °C for 24 h to determine their dry weight. Table 1 summarizes the range of environment conditions under which the experimental burns were conducted.

Table 1
Descriptive statistics for environmental variables associated with the Gestosa and Gondramaz experimental fires.

Variable	Average (St. dev)	Max	Min
Slope (degree)	13 (4)	24	4
Temperature (C)	18 (4)	24	10
RH (%)	57 (17)	80	26
6 m open wind speed (km h^{-1})	13 (10)	29	9
Live fuel moisture content (%) [a]	75 (23)	104	55
Dead fuel moisture content (%) [a]	10.3 (3.1)	16	7.4
	Gestosa/Gondramaz		
Fuel bed height (m)	0.97 (0.37)/0.29 (0.06)	1.64/0.35	0.5/0.25
Fuel load live (kg m^{-2})	1.15 (0.48)/0.5 (0.08)	2.03/0.64	0.6/0.46
Fuel load dead (kg m^{-2})	0.30 (0.13)/0.22 (0.11)	0.50/0.33	0.15/0.12
Fuel bulk density (kg m^{-3})	1.44 (0.53)/2.61 (0.70)	1.88/2.71	0.99/2.40

[a] Fuel moisture content on an ovendry weight basis.

2.3. Fire behaviour

2.3.1. Instrumentation

Local flame radiosity was measured using narrow angle radiometers (NAR) [12]. These radiometers are designed with a narrow field of view, verified experimentally to be a half-angle of 4.0°. The radiometers sense the equivalent flame radiosity occupying the conical volume defined by the radiometer's field of view (Fig. 1). Detailed description of the narrow angle radiometers is given in [12,24]. Radiometers were calibrated using a blackbody calibration source (Mikron M300, Mikron Instrument Company Inc., Oakland, NJ, USA) within the temperature range 380–1100 K (10–200 kW m^{-2}) with steps of 100 K. The narrow angle radiometers are calibrated to provide a measurement of flame radiosity at the location viewed by the radiometer. We assume that they provide a measurement of the flame radiosity averaged over the response of the sensor The radiometers showed a linear response within the calibration range and have a response time of nominally 30 ms. Based on the blackbody calibration source uncertainty the maximum NAR error was estimated to be approximately 3% at a temperature of 1300 K [15].

Flame gas temperature was measured with small diameter bare wire type K thermocouples (0.125 mm wire diameter/0.25 mm bead diameter – Omega Corporation, USA). Thermocouple measurements of flame temperatures are subject to errors induced by heat transfer between the thermocouple junction and its surroundings. Several authors discuss these sources of error (e.g., radiation gains and losses occurring respectively before and after the flame involves the thermocouple, conduction heat losses) and the necessary corrections to minimize them [14,25,26]. Nonetheless, the modification of the thermocouple surface properties as it is immersed in the flame fluid and the absence of fluid velocity measurements within the flame makes the application of these corrections impractical. The thermocouple size used represents a compromise between strength and size (large enough to survive installation and the turbulence yet small enough to minimize error due to radiative loss or gain). Thermocouple response time was nominally 150 ms for both heating and cooling. Calculations by Dupuy et al. [8], Hirano and Saito [13] and, Silvani and Morandini [14] estimated the uncertainty associated with these fine wire thermocouples to be between 5% and 7% of the measurement for a peak average temperature between 1200 and 1300 K, and flow velocities between 5 and 10 m s^{-1}.

Radiometer/thermocouple pairs were mounted along a 1.7 m tall tower, with sensors located at 0.6, 1.1 and 1.6 m above the ground. Figure 1 depicts a typical setup with all radiometers measuring radiation from the free flame. In some cases one or more sensors were located within the fuel layer. In this configuration the sensor was measuring radiation in the reaction zone. At each measuring height the radiometer was oriented horizontally and parallel to the direction of fire spread. The thermocouple was placed 0.1 m to the side of the radiometer sensor to minimize error due to instrument intrusiveness, such as the cooling of flame gases by the presence of the tower and radiometer encasing. The tower was insulated with an outer layer of 2.5 cm thick ceramic blanket and aluminium foil. The tower was placed vertically within the burn plot in a representative area of homogeneous fuel distribution, and connected to a datalogger (Campbell Scientific, Logan, UT, USA, model CR10X) buried in a shallow hole 2 m behind the tower. The instrument tower was located in an area that ensured

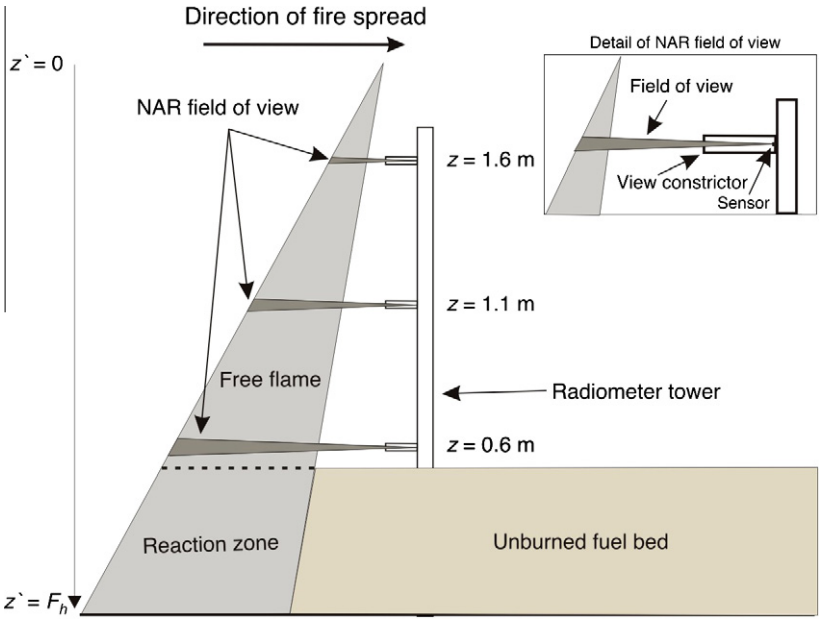

Fig. 1. Schematic of radiometer tower and detail of narrow angle radiometer (NAR) view of approaching flame.

the fire has gone through its acceleration stage and was spreading at its pseudo-steady state rate of spread when it reached the tower and there were no boundary effects, i.e., proximity to experimental plot edge. Tower placement and datalogger sheltering were accomplished to minimize disturbance to surrounding fuels. Data was acquired at 1 Hz. The radiometer tower was used in 15 burns. Data from four burns were discarded due to sensor damage caused by fire or deficient positioning of sensor tower.

2.3.2. Fire behaviour descriptors

Fires were ignited as a line source with drip torches ensuring a flame front spreading at a pseudo-steady rate of spread within 25 m of the ignition source. Fire behaviour information collected during the experimental fires and relevant for the present study included: rate of spread, fire intensity, residence time, and flame dimensions. Rate of spread was determined from oblique infrared (AGEMA THERMOVISION® 550) and visual cameras (SONY DCR-VX2000E PAL). Individual digitized frames were sampled at constant time intervals, varying typically from 30 s to 1 min depending on burn duration, and georeferenced using Computer-aided design (CAD) software (MicroStation 95). Flame front position was determined for each image frame, followed by rectification to a vertical plane to remove bias from the oblique view. The rectified images were then used to determine the rate of spread of the experimental fire. Fireline intensity (I_B), as defined by [26]:

$$I_B = R \cdot w_a \cdot h \quad (1)$$

with R being the fire rate of spread (m s^{-1}), w_a the fuel consumed in flaming combustion (kg m^{-2}), assumed to be all fuels (live and dead) with a diameter lower then 6 mm, and h the heat released by the combustion of fuel (assumed to be 18,600 kJ kg^{-1} for live and dead vegetation [17]). Residence time was derived from the time–temperature profiles measured in the experiments. Residence time was assumed to be the time the thermocouple temperature remained above 600 K (assumed as ignition temperature for vegetative fuels [27]) at the top of the fuel layer and indicates the presence of pyrolyzing flames. Flame depth (F_D) was inferred from the product of rate of spread and residence time. Flame height was estimated by averaging the flame dimension from digitized video frames and still photographs as the flame front passed the radiometer tower. For these measurements the radiometer tower was used as reference dimension.

Table 2
Basic fire behaviour information for shrubland experimental fires.

Plot	Rate of spread (m s^{-1})	Intensity (kW m^{-1})	Residence time (s)	Flame depth (m)	Flame height (m)
GE517	0.35	14,973	130	45.5	6
GE519	0.14	6808	86	11.7	5
GE523	–	–	35	–	1.5
GE527	–	–	21	–	2
GE600	0.06	1607	67	4.1	3.5
GE601	–	–	18	–	1.5
GE602	0.09	2342	67	6.1	2
GE613	0.08	2465	135	10.1	3.5
GO755	0.04	468	–	–	0.5
GO756	0.17	2228	44	7.6	1.75
GO758	0.06	543	21	1.2	0.75

GE – Gestosa; GO – Gondramaz.

Table 2 summarizes the basic fire behaviour characteristics for the 11 fires where radiosity and/or flame temperature data were collected. Rates of spread and fireline intensity varied between 0.04 and 0.35 m s^{-1}, 468 and 14,973 kW m^{-1} respectively. No reliable rate of fire spread data, and hence fireline intensity (Eq. (1)), were collected in three of the fires (plots 523, 527 and 601) due to instrument malfunction. Residence time varied between 18 and 135 s in the Gestosa experiments, and between 21 and 44 s in the Gondramaz experiments. Low residence time values, e.g., <30 s, were associated with low intensity burns (flame heights < 1.5), either no wind or flanking fires, whereas the high residence times were associated with experiments with fireline intensities higher then 2000 kW m^{-1}.

3. Results and discussion

3.1. General behaviour

Radiant energy emissions were collected in 11 experimental fires. In order to smooth local fluctuations in the flame radiosity

and fluid temperature data, the collected time series data were smoothed using a 5 s moving average. Figure 2a presents the instantaneous and smoothed radiosity traces measured at 1.1 m above ground in experimental fire GE602. The inset in this figure considers the distance between the flame and the sensor. This is based on the assumption of a constant rate of spread (Table 2), with negative distances indicating that the fire is moving toward the radiometer tower (located at distance = 0). Flame arrival was assumed to occur when the thermocouple measurement reached 600 K. Figure 2b presents the variation in radiosity at 0.6, 1.1 and 1.6 m for this experimental fire. The inset of this figure shows that the different NAR start sensing radiant energy fluxes at different distances from the flame. For this fire, the lower NAR senses the lowest radiosity until the flame front reaches the radiometer tower. This is explained by the existence of vegetation obstructing part of the field of view of the sensor while the flame front was some distance from the tower. Fuel bed height in this plot averaged 0.51 m, 0.09 m below the lower sensor (z = 0.6 m), but fuel heterogeneity result in a certain amount of shrubs with heights above 0.6 m. In this experiment the top NAR sensed significantly less energy than the middle NAR before the flame front arrived (Fig. 2b). This was caused by flame flickering, which made the flame to be occasionally out of the sensor field of view. Other factors contributing to the lower radiosity measured by the top NAR were, cooling due to entrainment and decreased flame depth with flame height.

As the fire reaches and immerses the NAR in hot fluid the sensors will warm and induce measurement errors. As the intent of the experiment was to quantify the flame radiosity, we were interested in the measurements performed immediately prior to and at flame immersion. Our measurement window excluded NAR measurements conducted 10 s after the arrival of the flame front. For plot 602, peak smoothed radiosity were 117, 125 and 105 kW m^{-2} respectively for sensors at a height of 0.6, 1.1 and 1.6 m. Table 3 presents peak flame radiosity measurements for the various fires.

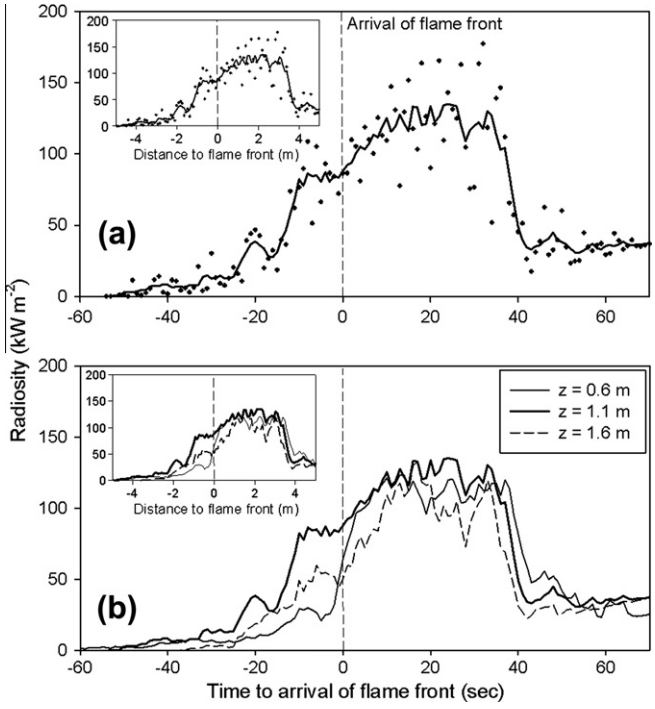

Fig. 2. Flame radiosity measured at experimental fire 602. (a) Plot of instantaneous (dots) and smoothed (moving average n = 5) radiosity measured at 1.1 m. (b) Plot of smoothed radiosity measured at 0.6, 1.1 and 1.6 m. Negative time values indicate fire approaching the radiometer sensor. Time = 0 indicates arrival of flame front to sensor. Inset x-axis assume constant rate of fire spread.

Table 3
Smoothed (n = 5) peak radiosity and temperature measured in Gestosa and Gondramaz shrubland fires.

Plot	Fuelbed height (m)	Peak radiosity (kW m^{-2})			Peak temperature (K)		
		Measurement height (m)					
		0.6	1.1	1.6	0.6	1.1	1.6
GE517	1.4	110.2	156.5	140.8	1177	1330	1198
GE519	1.2	169.6	110.8	175.7	1175	1124	1252
GE523	1.6	68.7	48.1	22	1094	841	666
GE527	1.2	94.9	92.4	77.9	747	804	794
GE600	0.9	112.1	157.7	161.3	1306	1283	1120
GE601	0.7	127.8	113.4	90.3	790	600	625
GE602	0.5	116.5	125.4	105.2	1241	1135	1144
GE613	1.1	sm	sm	sm	1198	936	1007
GO755	0.3	50.1	29.6	10.1	sm	613	577
GO756	0.4	51.7	30.6	11.8	1021	764	629
GO758	0.3	40.8	16.2	28.3	818	685	608

GE – Gestosa; GO – Gondramaz, sm – sensor malfunction.

3.2. Flame radiosity

Flame radiosity in the most intense fires were measured above 150 kW m^{-2}, reaching 161 and 176 kW m^{-2} in plot 519 and 600 respectively. Figure 3 depicts how the measured peak radiant energy flux varied with height above ground for each fire. The data do not identify a definite trend relative to how radiosity varies with height in the flame. The measurements in Table 3 and Fig. 3 are not directly comparable between fires as fuel bed height and fire characteristics are unique to each burn. The variety of fuel bed heights, ranging from 0.3 to 1.6 m meant that sensors at a given height were measuring distinct areas of the flame in different fires. As an example, in all the Gestosa burns but plot 602, the lower sensor was within the reaction zone, whereas for the Gondramaz plots all sensors were measuring radiosity within the free flame (Table 3). In Gondramaz 755 and 758 the top NAR was measuring radiation above the estimated average flame height, hence above the perceived visual flame height.

The low peak radiosity measured in the Gondramaz burns (between 41 and 52 kW m^{-2}) were associated with short and narrow flames derived from low fuel availability for combustion (a combination of lower fuel load and high fuel moisture content). The fires in Fig. 3 with a maximum measured radiosity lower than 125 kW m^{-2} had flame heights lower than 2 m. These fires show an overall decrease in radiosity with height. In this experiments the top narrow angle radiometer (z = 1.6 m) was sensing an area of intermittent flame presence. In the experimental fires with

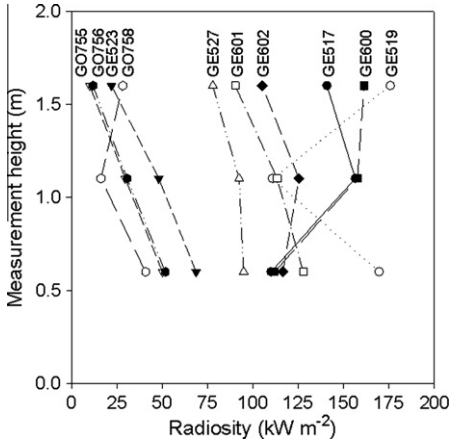

Fig. 3. Peak radiosity variation with height (m) above ground for shrubland experimental fires. Numerals indicate plot number.

flame heights higher then 3 m (e.g., Gestosa 517, 519 and 600) an observable increase in peak radiosity occurred from the 0.6 m sensor to the sensors above. This was likely to occur because the lower measurements were well within the gaseous fuel rich environment of the reaction zone in deep flames. For these burns the measurements at 1.6 m were just above the fuel layer height, where optimal fuel – oxidizer mixing would occur. This suggests that for high intensity flames the oxidizer limited environment of the reaction zone restricts the radiant energy output within the fuel layer and peak radiant flux emission occurs in the free flame above it.

Only a few studies report measurements of flame radiosity in spreading fires. [11,12] applied narrow angle radiometers in shallow fuel layers in a laboratory setting. These laboratory fires were conducted under a range of burning conditions with maximum mean flame heights attained around 2 m tall. These authors measured radiant energy fluxes comparable to the ones attained in our study in which flame heights were lower than 2 m. [11] reported peak radiative emissive power of 90 kW m^{-2} for experiments with flame heights of 2–2.2 m; whereas [12] measured peak values of 60 kW m^{-2}, for flames 1–1.5 m tall. [11] also quantified a decrease in radiation intensity in the free flame with height. Our results for fires with flames smaller then 2 m in Fig. 3 shows similar trend. Silvani and Morandini [14] measured radiant heat fluxes peaking at 51 kW m^{-2} on the top of the fuel array in 0.8 m tall shrubs. Their values are consistent with our measurements obtained in short and narrow flames.

Butler et al. [15] measured radiosity in experimental crown fires, where peak flame radiant energy fluxes surpassed 250 kW m^{-2} in the most intense fire. By relying on two 13.8 m tall towers instrumented with narrow angle radiometers, [15] was able to capture both the vertical profile and horizontal variability in radiosity. Their measurements suggest that the horizontal variability in flame radiosity is comparable to the vertical variability when considering the flame profile between the ground and the top of the canopy fuel layer. By averaging the vertical flame profile of 6 experimental burns their results suggest a constant peak radiant energy flux within the subcanopy and canopy space, which could be considered the reaction zone of an active crown fire. These results agree with our measurements of radiant energy flux within the reaction zone in shrubland fires. Considering the group of fires with flame heights above 3 m, the average radiosity was 103, 105 and 101 kW m^{-2} for 0.6, 1.1 and 1.6 m height, respectively. As for [15] our measurements in the tall and deep flames were limited by the relative small dimension of our tower relative to the observed flame heights. For these burns we were unable to capture the radiant energy profile of the upper free flame.

Wotton et al. [11] considered that flame radiative characteristics follow a consistent pattern as a function of the distance from the flame tip ($z' = 0$ in Fig. 1). This hypothesis considers that flames of distinct heights, e.g., 1 and 2 m tall, will yield comparable radiant energy fluxes at the same distance below the flame tip. We analysed flame profile data considering: (1) the NAR measurement location as a vertical distance from the tip of the flame (following [11]); and (2) a nondimensional approach with the average flame height to vary between 0 (visual flame tip) and 1 (lower boundary of reaction zone, i.e., the ground). Figure 4a and b shows the vertical profile of flame radiosity as a distance from the flame tip for the data in Table 2. The data in Fig. 4 shows considerably larger scatter than that found by Wotton et al. [11] for laboratory fires burning under zero wind. This is likely to be the result of several factors, namely the larger range in flame heights measured in our experiments, the nonsteady ambient wind speed and localized flame

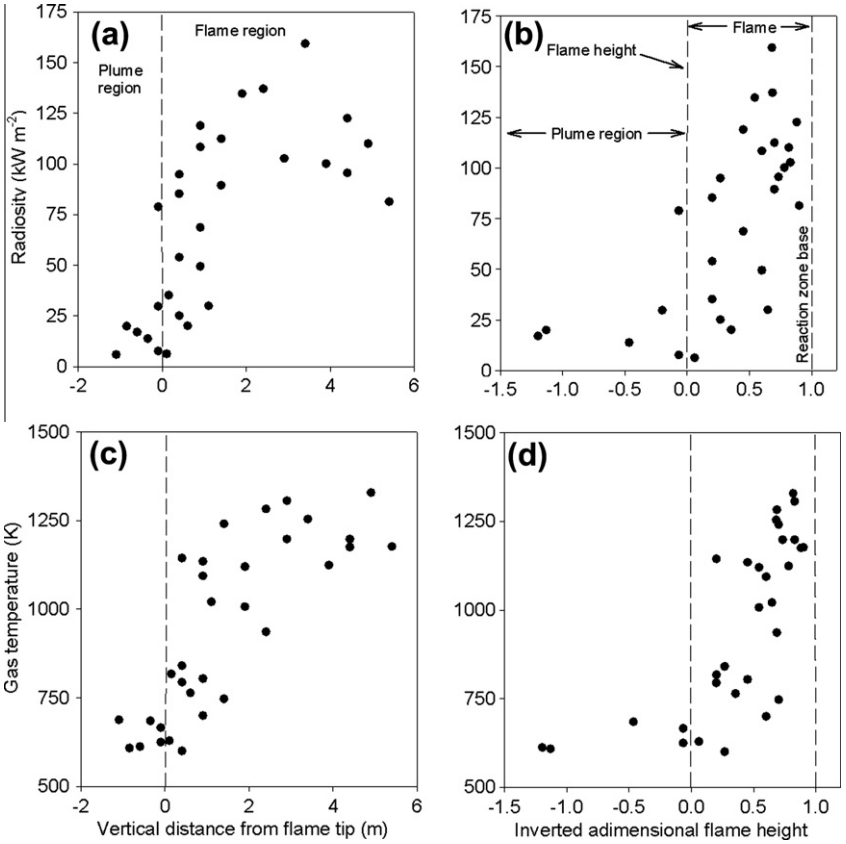

Fig. 4. Flame vertical profile characteristics. (a and c) Peak radiosity and maximum temperature as a function of vertical distance from flame tip. 0 is flame tip; positive numbers indicate distance from tip towards flame base. (b and d) Peak radiosity and maximum temperature as a function of nondimensional position in flame vertical profile. 0 is located at flame tip and 1 at lower boundary of reaction zone, i.e., the ground.

front–atmosphere interactions that results in highly turbulent flame flow. Analysis of the variation in flame characteristics considering the nondimensional flame profile shows a linear variation in flame characteristics.

3.3. Flame temperature

Smoothed ($n = 5$) peak flame temperatures varied between 1200 and 1300 K in the experiments with flame height higher then 3 m, and 750–1000 K in experiments with flame heights lower then 2 m. The lower flame temperature (i.e., <700 K) data in Table 3 originates from thermocouples located within the intermittent flame and plume region (Fig. 4c). It is felt that the relatively low sampling rate (1 Hz) limits the inferences that can be made from the fires with smaller flame residence times, i.e., <30 s. Peak gas temperatures were significantly correlated with peak radiosity (Pearson's $r = 0.73$). Peak flame temperatures correlated with flame size, i.e., height and depth, and the measurement location in the flame (reaction zone, free flame or intermittent flame region). Within the subset of experiments with flame heights above 3 m flame temperature measurements were concentrated in the rich and persistent flame regions. In these regions of the flame the measurements did not show an increase in flame temperature with flame depth and/or height; temperatures seem to asymptote to 1250 K (Fig. 4c). The highest flame temperatures were measured in the interface between the reaction zone and the free flame (Table 2). The data showed a noticeable decrease of flame temperature in its last meter, the area of intermittent flame (Fig. 4c). Our results indicate flame tip temperatures between 600 and 800 K, with the large variability in flame temperature around the flame tip associated with the variability in flame structure due to its turbulent nature and the inherent difficulty in estimating flame height. A plot of flame temperature as a function of the adimensional location within the flame (Fig. 4b) shows a linear decrease in temperature with proximity of the flame tip.

Our peak flame temperatures were consistent with measurements obtained in the persistent flame region in laboratory [8,11,28] and outdoor shrubland fires [18]. Our peak flame temperatures were somewhat lower then measured within the rich and flame region of high intensity crown fires [15] and [29]. These authors report maximum temperatures averaging 1450 K. The rich and persistent flame regions in these experimental fires were characterized by a consistent maximum flame temperature [30]. This is comparable to our results (Fig. 4c).

4. Conclusions

A series of outdoor experimental fires in shrubland fuels conducted under variable fuel (e.g., fuel layer bulk density and load, fuel moisture content) and fire environment conditions (e.g., slope, air temperature, relative humidity, wind speed) provided quantitative data on flame radiant energy flux and temperature profiles over a range of flame sizes. Our measurements showed that flame radiosity vary considerably with flame structure and size. Our higher intensity burns yielded peak radiant energy fluxes between 150 and 175 kW m^{-2} and flame gas kinetic temperatures between 1200 and 1330 K. The dataset identified a radiometric gradient within the vertical dimension of the shrubland flames. This radiometric profile was characterized by no change in energy flux within the reaction zone and the lower portion of the free flame, followed by decay as the measurement location approached the flame tip. Measurements of radiative energy flux at the flame tip showed the highest variability, likely due to the pulsating nature of the flame, and its intermittent presence in the conical volume element targeted by the narrow angle radiometers. In an outdoor setting, with variable wind speed and direction, the fluctuating nature of the flame is amplified compared to what is observed in a controlled laboratory environment.

The comparison of our results with experimental measurements of flame radiant energy flux in laboratory and high intensity experimental crown fires reveal the significance of scale in quantifying fundamental fire phenomena. Our radiant energy flux measurements were substantially higher than measurements obtained within a laboratory setting, and lower than found in active crown fires. Peak gas temperatures in the flame seemed to not be as affected by scale. Our measurements were consistent with those reported from laboratory and outdoor experimental fires [11,12,15].

The present dataset constitutes a unique description of fundamental flame properties that provide insight into flame dynamics and heat transfer phenomena. The dataset has further use to calibrate and evaluate physical model components.

Acknowledgments

Many individuals were involved in the experimental burn program throughout the years, namely L.M. Ribeiro, L.P. Pita, S. Cardoso, A. Trindade, and N. Luis, from Associação para o Desenvolvimento da Aerodinâmica Industrial. Their contribution to the preparation and execution of experimental burns is gratefully acknowledged. The support of Direccao Geral de Florestas by making the Gestosa and Gondramaz sites available for the experimental burning program is acknowledged. Thanks to the voluntary fire fighting units (Bombeiros Voluntarios (BV) Castanheira de Pera, BV Lousa, and BV Miranda do Corvo) that provided suppression resources during the preparation and execution of the experimental burns. Thanks also to Kyle Shannon for preparing and calibrating some of the experimental equipment.

References

[1] R.R. Linn, Transport Model for Prediction of Wildfire Behavior, Los Alamos National Laboratory Scientific Report LA13334-T, 1997.
[2] B. Porterie, D. Morvan, J.C. Loraud, M. Larini, Phys. Fluids 12 (2000) 1762–1782.
[3] D. Morvan, J.L. Dupuy, Combust. Flame 127 (2001) 1981–1994.
[4] O. Sero-Guilaume, J. Margerit, Int. J. Heat Mass Transfer 45 (2002) 1705–1722.
[5] E.A. Catchpole, N. de Mestre, Aust. Forest. 49 (1986) 102–111.
[6] R.O. Weber, Proc. Energy Combust. Sci. 17 (1991) 67–82.
[7] J.M.C. Mendes-Lopes, J.M.P. Ventura, J.M.P. Amaral, Int. J. Wildland Fire 12 (2003) 67–84.
[8] J.L. Dupuy, J. Marechal, D. Morvan, Combust. Flame 135 (2003) 65–76.
[9] X. Zhou, L. Sun, S. Mahalingam, D.R. Weise, Combust. Sci. Technol. 175 (2003) 1293–1316.
[10] J.L. Dupuy, P. Vachet, J. Marechal, J. Melendez, A.J. Castro, Int. J. Wildland Fire 16 (2007) 324–340.
[11] M.B. Wotton, T.L. Martin, K. Engel, Vertical flame intensity profile from a surface fire, in: Proc. 13th Conference on Fire and Forest Meteorology, Lorne, Victoria, Australia, 1998.
[12] B.W. Butler, Experimental measurements of radiant heat fluxes from simulated wildfire flames, in: Proc. 12th Conference on Fire and Forest Meteorology, Jekyll Island, Georgia, 1994.
[13] T. Hirano, K. Saito, Prog. Energy Combust. Sci. 20 (1994) 461–485.
[14] X. Silvani, F. Morandini, Fire Safe. J. 44 (2009) 279–285.
[15] B.W. Butler, J. Cohen, D.J. Latham, R.D. Schuette, P. Sopko, K.S. Shannon, D. Jimenez, L.S. Bradshaw, Can. J. Forest. Res. 34 (2004) 1577–1587.
[16] B.J. Stocks, M.E. Alexander, B.M. Wotton, C.N. Stefner, M.D. Flannigan, S.W. Taylor, N. Lavoie, J.A. Mason, G.R. Hartley, M.E. Maffey, G.N. Dalrymple, T.W. Blake, M.G. Cruz, R.A. Lanoville, Can. J. Forest. Res. 34 (2004) 1548–1560.
[17] F.A. Albini, Fizika Goreniya i Vzriva 32 (1996) 71–82 (in English) translated journal is printed in english as "Physics of Combustion, Explosion and Shock Waves".
[18] P.A. Santoni, A. Simeoni, J.L. Rossi, F. Bosseur, F. Morandini, X. Silvani, J.H. Balbi, D. Cancellieri, L. Rossi, Fire Safe. J. 41 (2006) 171–184.
[19] D.X. Viegas, P.M. Palheiro, L.P. Pita, L.M. Ribeiro, M.G. Cruz, A Ollero, B. Arrue, M. Ramiro, Analysis of fire behaviour in Mediterranean shrubs: the Gestosa fire experiments (Portugal), in: Proc 5th International Conference on Forest Fire Research, Figueira da Foz, Portugal, 2006
[20] W.R. Catchpole, C.J. Wheeler, Aust. J. Ecol. 17 (1992) 121–131.
[21] R.H. Canfield, J. Forest. 39 (1941) 388–394.

[22] M.G. Cruz, D.X. Viegas, 1998. Fire behavior in some common Central Portugal fuel complexes: Evaluation of fire behavior models performance, in: Proc 3rd International Conference on Forest Fire Research–14th Conference on Fire and Forest Meteorology, Luso, Portugal, 1998.
[23] P.M. Fernandes, W.R. Catchpole, F.C. Rego, Can. J. Forest. Res. 30 (2000) 889–899.
[24] B.W. Butler, Field measurements of radiant energy transfer in full scale wind driven crown fires, in: Proc. 6th ASME–JSME Thermal Engineering Joint Conference, 2003.
[25] C.R. Shaddix Practical aspects of correcting thermocouple measurements for radiation loss, in: Proc. 1998 Fall Meeting of Western States Section, The Combustion Institute, University of Washington, Seattle, WA, 1998.
[26] K.S. Shannon, B.W. Butler, A review of error associated with thermocouple temperature measurement in fire environments, in: Proc. 2nd International Fire Ecology and Fire Management Congress, November 2003, Orlando, FL, 2003.
[27] G.M. Byram, in: K.P. Davis (Ed.), Forest Fire: Control and Use, McGraw-Hill Book Company, New York, 1959. pp. 61–89, 554–555.
[28] F.A. Albini, B.J. Stocks, Combust. Sci. Technol. 48 (1986) 65–76.
[29] P.A. Santoni, T. Marcelli, E. Leoni, Combust. Flame 131 (2002) 47–58.
[30] S.W. Taylor, B.M. Wotton, M.E. Alexander, G.N. Dalrymple, Can. J. Forest. Res. 34 (2004) 1561–1576.